

Free Isotropic-Nematic Interfaces in Fluids of Charged Platelike Colloids

Markus Bier,* Ludger Harnau, and S. Dietrich

*Max-Planck-Institut für Metallforschung,
Heisenbergstraße 3, 70569 Stuttgart, Germany,
and*

*Institut für Theoretische und Angewandte Physik,
Universität Stuttgart, Pfaffenwaldring 57, 70569 Stuttgart, Germany*

(Dated: June 14, 2005)

Bulk properties and free interfaces of mixtures of charged platelike colloids and salt are studied within density-functional theory. The particles are modeled by hard cuboids with their edges constrained to be parallel to the Cartesian axes corresponding to the Zwanzig model. The charges of the particles are concentrated in their center. The density functional is derived by functional integration of an extension of the Debye-Hückel pair distribution function with respect to the interaction potential. For sufficiently small macroion charges, the bulk phase diagrams exhibit one isotropic and one nematic phase separated by a first-order phase transition. With increasing platelet charge, the isotropic and nematic binodals are shifted to higher densities. The Donnan potential between the coexisting isotropic and nematic phases is inferred from bulk structure calculations. Non-monotonic density and nematic order parameter profiles are found at a free interface interpolating between the coexisting isotropic and nematic bulk phases. Moreover, electrically charged layers form at the free interface leading to monotonically varying electrostatic potential profiles. Both the widths of the free interfaces and the bulk correlation lengths are approximately given by the Debye length. For fixed salt density, the interfacial tension decreases upon increasing the macroion charge.

PACS numbers: 61.20.Qg, 61.20.Gy, 61.30.Gd, 61.70.Md

Keywords: charged platelike colloids; inhomogeneous multicomponent fluids; anisotropic particles; Donnan potential; density-functional theory; isotropic-nematic coexistence; free interfaces

I. INTRODUCTION

Platelike colloidal particles play a decisive, constitutive role in processes like agriculture, construction, oil drilling, or coating. This wide range of applicability mirrors a very rich phase behavior of suspensions of platelets, including liquid crystalline phases, sol-gel transitions, and flocculation, depending on numerous material parameters, like size, shape, or charge of the particles, as well as on effective, solvent mediated interactions which can be tuned, e.g., by the choice of the solvent, salt concentration, or pH-value. Whereas bulk properties of suspensions of charged platelets have been investigated for decades [1], free interfaces between coexisting fluid phases in such systems have not yet been studied. Here we focus on this latter issue by proposing and studying a density-functional theory of such inhomogeneous multicomponent systems of charged anisotropic particles.

On the experimental side, characterization of bulk phases have been conducted for several model systems like natural clay [2, 3], laponite [4, 5, 6, 7, 8, 9, 10, 11, 12, 13, 14], sterically stabilized gibbsite [15, 16, 17, 18], or nickel(II)hydroxide [19, 20] using methods like polarized light analysis [5, 15, 16, 17, 18], light scattering [7, 11, 12], small-angle scattering with neutrons or x-rays [4, 6, 7, 9, 19, 20], rheological measurements [4, 8, 10], or NMR [13, 14]. Since coexistence between bulk phases of

charged gibbsite platelets has already been observed experimentally [17, 18], we expect that the spatially varying structural properties between them are also experimentally accessible using, e.g., scattering [21] or optical [22] techniques.

The theoretical description of suspensions of charged platelets is rather complicated due to long-ranged, anisotropic interactions and many different length scales. Interfaces and surfaces in such systems add further difficulties induced by the partial loss of translational symmetry. Under these circumstances it is advisable to start with simplified models. In the presented one, the particles are modeled as hard cuboids with pointlike charges concentrated in their center. Furthermore, the platelet orientations are restricted to three mutually perpendicular directions, which is commonly known as the Zwanzig model [23]. Finally, in order to gain computational advantages, distances between particles are not measured by the usual Euclidean norm but by the so-called supremum norm.

Density-functional theory [24] is a very effective method to investigate inhomogeneous fluid systems. It has recently been applied to describe suspensions of platelets with pure hard-core interactions near interfaces and surfaces [25, 26, 27]. Here we study platelets interacting via a hard-core plus a Coulomb potential; further interactions like dispersion forces are not considered, which corresponds to a suspension in which the indices of refraction between solvent and solute are matched. The density functional is constructed by functional integration of the two-particle density with respect to the

*Electronic address: bier@fluids.mpi-stuttgart.mpg.de

interaction potential [24], which is the analogue to a Debye-charging process [28]. The two-particle density can be obtained, e.g., by interaction site model calculations [29, 30] or expressed in terms of the potential of mean force which may be approximated by effective pair potentials [31, 32, 33]. For reasons of computational advantages, here we choose an extension of the even simpler Debye-Hückel pair distribution function [28] in which the Debye screening factor is replaced by a spatially varying quantity.

In view of these approximations, this theoretical model can be expected to be only qualitatively correct. The most subtle point is the choice of the pair distribution function, which requires further improvements in order to increase the quantitative reliability. However, the other parts of the formalism are expected to remain valid and thus provide the basis for future efforts. In this sense, the following sections present a generic formalism for free interfaces in fluids of charged platelike colloids, implemented exemplarily for the above-mentioned extended Debye-Hückel pair distribution function.

The text is structured as follows. In Sec. II the general formalism with a detailed derivation of the actual density functional is presented. Section III is devoted to bulk phase diagrams of the model. The structures of free interfaces between an isotropic and a nematic bulk phase are calculated in Sec. IV. Section V discusses the current approach and summarizes our results.

II. GENERAL FORMALISM

A. Definitions

We consider a ternary mixture of charged hard square cuboids with their edges required to be parallel to the Cartesian axes (Zwanzig model [23]) dissolved in a dielectric solvent (e.g., water) with dielectric constant ϵ . The solvent is treated as a continuum. For simplicity, the charges are fixed, monodisperse, and concentrated in the centers of the particles. The particles of the first component, representing the macroions M, have size $D_M \times D_M \times L_M$, $D_M \neq L_M$, and charge $Q_M \leq 0$. Within the Zwanzig approximation, macroions can take three different orientations, denoted as M_x , M_y , or M_z corresponding to whether the L_M -edges are parallel to the x -, y -, or z -axis, respectively (see Fig. 1). The second component consists of salt anions A modeled as cubes of side length $D_A := D_S$ and charge $Q_A := Q_S < 0$ (see Fig. 1). Finally, the third component consists of salt cations C and counterions guaranteeing overall charge neutrality. They are also described by cubes with the same side length $D_C := D_S$ but opposite charge $Q_C := -Q_S > 0$ (see Fig. 1).

We denote as $\varrho_i(\mathbf{r})$, $i \in \{M_x, M_y, M_z, A, C\}$, the number density at point \mathbf{r} of the centers of macroions with orientation $M_{x,y,z}$, anions, and cations, respectively. Note that the position $\mathbf{r} \in V \subseteq \mathbb{R}^3$, with V denoting the

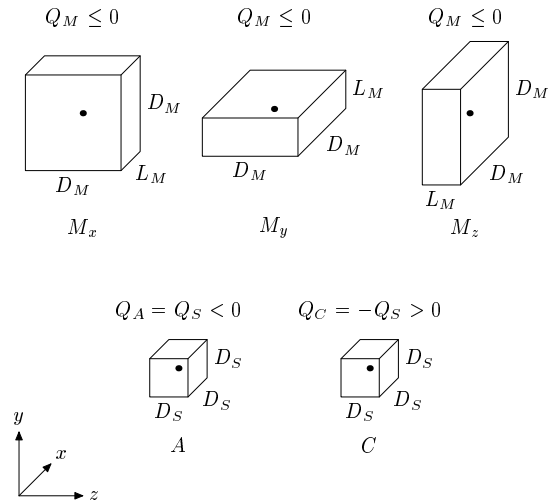
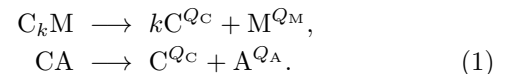


FIG. 1: Macroions M are square cuboids of size $D_M \times D_M \times L_M$, $D_M \neq L_M$ with charge Q_M , whereas anions A and cations C are cubes of side length D_S with charges Q_S and $-Q_S$, respectively. The pointlike charges (\bullet) are localized in the centers of the cuboids. The macroions can adopt three possible orientations M_x , M_y , and M_z corresponding to the L_M -edges being parallel to the x -, y -, and z -axis, respectively.

system volume, is a *continuous* variable in contrast to the orientation of macroions, which varies within a *discrete* set. As an abbreviation, we introduce $\underline{\varrho}(\mathbf{r}) := (\varrho_{M_x}(\mathbf{r}), \dots, \varrho_C(\mathbf{r}))$.

The system under consideration is coupled to two particle reservoirs: One supplies neutralized macroions (chemical formula $C_k M$, $k := \frac{Q_M}{Q_S}$) and the other neutral salt (chemical formula CA); $\mu_{C_k M}$ and μ_{CA} denote the corresponding chemical potentials. Upon entering the solvent, these molecules dissociate:



These equilibrium chemical reactions lead to the following relations between the reservoir chemical potentials ($\mu_{C_k M}$ and μ_{CA}) and the particle chemical potentials (μ_i , $i \in \{M_x, M_y, M_z, A, C\}$, $\mu_{M_x} = \mu_{M_y} = \mu_{M_z}$):

$$\begin{aligned} \mu_{C_k M} &= k \mu_C + \mu_{M_{x,y,z}}, \\ \mu_{CA} &= \mu_C + \mu_A. \end{aligned} \quad (2)$$

B. Density-functional theory

The configurations of this system are characterized by the set of number density profiles $\underline{\varrho}$. The equilibrium states minimize the grand canonical density functional [24, 34]

$$\Omega[\underline{\varrho}] = \sum_i \int_V d^3r \varrho_i(\mathbf{r}) (\ln \varrho_i(\mathbf{r}) - 1 - \mu_i^*) + F^{\text{ex}}[\underline{\varrho}], \quad (3)$$

where F^{ex} is the free energy in excess over the ideal gas contribution. Here, the reduced particle chemical potentials $\mu_i^* := \mu_i - \ln(\Lambda_i^3)$ with the thermal de Broglie wavelength Λ_i ($\Lambda_{M_x} = \Lambda_{M_y} = \Lambda_{M_z}$) for particles of class i have been introduced. With the reduced reservoir chemical potentials

$$\begin{aligned}\mu_{C_kM}^* &:= \mu_{C_kM} - \left(\ln(\Lambda_{M_{x,y,z}}^3) + k \ln(\Lambda_C^3) \right) \\ \mu_{CA}^* &:= \mu_{CA} - \left(\ln(\Lambda_A^3) + \ln(\Lambda_C^3) \right),\end{aligned}\quad (4)$$

Eq. (2) takes the form

$$\begin{aligned}\mu_{C_kM}^* &= k\mu_C^* + \mu_{M_{x,y,z}}^* \\ \mu_{CA}^* &= \mu_C^* + \mu_A^*.\end{aligned}\quad (5)$$

For given reservoir chemical potentials $\mu_{C_kM}^*$ and μ_{CA}^* , the particle chemical potentials μ_i^* are fixed by Eq. (5) and the constraint of global charge neutrality:

$$\int_V d^3r \sum_i Q_i \varrho_i(\mathbf{r}) = 0. \quad (6)$$

The Euler-Lagrange equations of the minimization problem read

$$\frac{\delta \Omega}{\delta \varrho_i(\mathbf{r})} = \ln(\varrho_i(\mathbf{r})) - \mu_i^* - c_i(\mathbf{r}) = 0 \quad (7)$$

with the one-particle direct correlation function

$$c_i(\mathbf{r}) := -\frac{\delta F^{\text{ex}}}{\delta \varrho_i(\mathbf{r})}.$$

If $\underline{\varrho} = \underline{\varrho}^{\text{eq}}$ minimizes the density functional in Eq. (3), the grand potential $\Omega(T, V, \mu_{C_kM}^*, \mu_{CA}^*) = -p(T, V, \mu_{C_kM}^*, \mu_{CA}^*)V$ with the osmotic pressure $p(T, V, \mu_{C_kM}^*, \mu_{CA}^*)$ equals $\Omega[\underline{\varrho}^{\text{eq}}]$. Phase coexistence corresponds to different states with equal values of the pressure p , the chemical potential $\mu_{C_kM}^*$ of the reservoir of neutralized platelets, and the chemical potential μ_{CA}^* of the salt reservoir. In particular, coexistence does *not* imply equal values of the particle chemical potentials μ_i^* , $i \in \{M_x, M_y, M_z, A, C\}$. Rather, coexisting bulk phases give rise to a Donnan potential maintaining different chemical potentials μ_i^* .

C. Excess free energy

The above considerations are valid for any interaction between the particles. In this subsection, our choice of the model and the resulting excess free energy F^{ex} are specified.

The interaction energy $U_{ij}(\mathbf{r}, \mathbf{r}')$ of a particle of class i at position \mathbf{r} with a particle of class j at position \mathbf{r}' comprises a hard-core potential $U_{ij}^h(\mathbf{r}, \mathbf{r}')$, which prevents the particles from overlapping, and a contribution $U_{ij}^c(\mathbf{r}, \mathbf{r}')$ due to the charges: $U = U^h + U^c$. As stated in the Introduction (Sec. I), we do not consider dispersion forces.

The interactions between the charges are approximated as

$$U_{ij}^c(\mathbf{r}, \mathbf{r}') := \frac{Q_i Q_j}{\|\mathbf{r} - \mathbf{r}'\|_\infty}, \quad (9)$$

where the usual Euclidean norm $\|\mathbf{r}\|_2 = \sqrt{x^2 + y^2 + z^2}$ is replaced by the supremum norm $\|\mathbf{r}\|_\infty = \max(|x|, |y|, |z|)$ because of computational advantages. Since these two norms are equivalent, i.e., $\|\mathbf{r}\|_\infty \leq \|\mathbf{r}\|_2 \leq \sqrt{3} \|\mathbf{r}\|_\infty$, we do not expect that the results change qualitatively due to this approximation. Furthermore, $\|\cdot\|_\infty$ -spheres are cubes with their edges parallel to the Cartesian axes; therefore, the supremum norm is the most natural and adapted norm in the context of a Zwanzig model for cuboids.

As described in Ref. [24], the exact relation

$$\frac{\delta F^{\text{ex}}}{\delta U_{ij}(\mathbf{r}, \mathbf{r}')} = \frac{1}{2} \varrho_i(\mathbf{r}) \varrho_j(\mathbf{r}') g_{ij}(\mathbf{r}, \mathbf{r}') \quad (10)$$

with the pair distribution function g corresponding to the pair potential U can be functionally integrated along the path $U^{(\eta)} := U^h + \eta U^c$, $\eta \in [0, 1]$, which yields

$$\begin{aligned}F^{\text{ex}}[\underline{\varrho}] &= F^{\text{ex,h}}[\underline{\varrho}] + \frac{1}{2} \sum_{ij} \int_V d^3r \int_V d^3r' \\ &\varrho_i(\mathbf{r}) \varrho_j(\mathbf{r}') U_{ij}^c(\mathbf{r}, \mathbf{r}') \int_0^1 d\eta g_{ij}^{(\eta)}(\mathbf{r}, \mathbf{r}'),\end{aligned}\quad (11)$$

where $F^{\text{ex,h}}$ is the excess free energy corresponding to the pure hard-core potential U^h , and $g^{(\eta)}$ denotes the (inhomogeneous) pair distribution function for the pair potential $U^{(\eta)}$. $F^{\text{ex,h}}$ is chosen as the fundamental measure functional introduced by Cuesta and Martínez-Ratón [35, 36]:

$$F^{\text{ex,h}}[\underline{\varrho}] := \int_V d^3r \Phi(\underline{n}(\mathbf{r})) \quad (12)$$

with the weighted densities

$$n_\alpha(\mathbf{r}) = \sum_i \int_V d^3r' \omega_{\alpha,i}(\mathbf{r} - \mathbf{r}') \varrho_i(\mathbf{r}') \quad (13)$$

for $\alpha \in \{0, 1x, 1y, 1z, 2x, 2y, 2z, 3\}$ and the excess free energy density

$$\Phi(\underline{n}) = -n_0 \ln(1 - n_3) + \sum_{q \in \{x,y,z\}} \frac{n_{1q} n_{2q}}{1 - n_3} + \frac{n_{2x} n_{2y} n_{2z}}{(1 - n_3)^2}. \quad (14)$$

Due to Eq. (9), the η -integration in Eq. (11) may be interpreted as a Debye charging process [28, 37]. This motivates to approximate $g^{(\eta)}$ by an expression similar to

the pair distribution function of the Debye-Hückel theory [28, 37, 38, 39]:

$$g_{ij}^{(\eta)}(\mathbf{r}, \mathbf{r}') := \exp(-U_{ij}^h(\mathbf{r}, \mathbf{r}')) \max[0, 1 - U_{ij}^c(\mathbf{r}, \mathbf{r}')] \times \eta \exp(-\sqrt{\eta}\kappa(\mathbf{r}, \mathbf{r}'; [\underline{\rho}]) \|\mathbf{r} - \mathbf{r}'\|_\infty). \quad (15)$$

This pair distribution function has non-negative values, it vanishes within the hard-core, and it approaches unity at infinitely large distances. Again, here the Euclidean norm $\|\cdot\|_2$ has been replaced by the supremum norm $\|\cdot\|_\infty$. The factor $\sqrt{\eta}$ in Eq. (15) is introduced because in a Debye charging process all charges Q_i are replaced by $\sqrt{\eta}Q_i$. Furthermore, the charges Q_i have to be interpreted as effective charges in order to reproduce the actual effective interactions between charged particles within Debye-Hückel theory [40].

The screening factor κ in Eq. (15) is chosen as

$$\kappa(\mathbf{r}, \mathbf{r}'; [\underline{\rho}]) := \frac{1}{2} (\tilde{\kappa}(\mathbf{r}; [\underline{\rho}]) + \tilde{\kappa}(\mathbf{r}'; [\underline{\rho}])) \quad (16)$$

where only anions and cations contribute to the screening [41]:

$$\tilde{\kappa}(\mathbf{r}; [\underline{\rho}]) := \sqrt{4\pi Q_S^2 (\varrho_A(\mathbf{r}) + \varrho_C(\mathbf{r}))}. \quad (17)$$

Our analysis rendered that, for a spatially constant screening factor κ , the above model does not yield stable interfacial profiles. This led us to introduce the spatially varying expression in Eq. (16). Alternative expressions for inhomogeneous screening factors are known from the theory of electrolytes: In Refs. [39, 42] non-symmetric screening factors are provided whereas in Ref. [43] κ is calculated from the mean salt density. We prefer the definition in Eqs. (16) and (17) because it is symmetric and the screening is determined by the salt concentration *at* the actually investigated positions.

The expansion of $\Omega[\underline{\rho} = \underline{\rho}^{(\text{hom})} + \delta\underline{\rho}]$ around a spatially homogeneous state $\underline{\rho}^{(\text{hom})}$ in powers of perturbations $\delta\underline{\rho}$ shows that the spatially homogeneous state $\underline{\rho}^{(\text{hom})}$ is unstable with respect to spatial variations if the macroion charge $|Q_M|$ is sufficiently large because the second order term can become negative. Thus, the choice for $g^{(\eta)}$ in Eq. (15) leads to spatially *inhomogeneous* bulk phases if the macroion charge $|Q_M|$ is larger than some threshold value. Here, we restrict ourselves to the case of spatially *homogeneous* bulk phases, i.e., only sufficiently small macroion charges are considered.

With Eq. (15), the innermost integral in Eq. (11) can be evaluated leading to an expression

$$\int_0^1 d\eta g_{ij}^{(\eta)}(\mathbf{r}, \mathbf{r}') \quad (18)$$

$$= \exp(-U_{ij}^h(\mathbf{r}, \mathbf{r}')) (1 + G_{ij}(\kappa(\mathbf{r}, \mathbf{r}'; [\underline{\rho}]), \|\mathbf{r} - \mathbf{r}'\|_\infty))$$

with functions

$$G_{ij}(\kappa, s) := - \int_0^1 d\eta \min[1, U_{ij}^c(s)\eta \exp(-\sqrt{\eta}\kappa s)] \quad (19)$$

which decay for $s \rightarrow \infty$ as

$$\begin{aligned} G_{ij}(\kappa, s) &\simeq - \int_0^1 d\eta U_{ij}^c(s)\eta \exp(-\sqrt{\eta}\kappa s) \\ &= - \frac{Q_i Q_j}{s} \int_0^1 d\eta \eta \exp(-\sqrt{\eta}\kappa s) \\ &= - \frac{Q_i Q_j}{s} \int_0^1 d\zeta 2\zeta^3 \exp(-\zeta\kappa s) \\ &= - \frac{2Q_i Q_j}{\kappa^4 s^5} \gamma(4, \kappa s) \\ &\simeq - \frac{12Q_i Q_j}{\kappa^4 s^5}, \end{aligned} \quad (20)$$

where γ denotes the incomplete gamma function [44, 45]. Therefore, the integrand in Eq. (11) vanishes at small distances $\|\mathbf{r} - \mathbf{r}'\|_\infty$ due to U_{ij}^h , whereas it decays as $\|\mathbf{r} - \mathbf{r}'\|_\infty^{-1}$ for $\|\mathbf{r} - \mathbf{r}'\|_\infty \rightarrow \infty$. In order to isolate the $\|\mathbf{r} - \mathbf{r}'\|_\infty^{-1}$ asymptotics, we add and subtract unity on the right-hand side of Eq. (18), which, after insertion into Eq. (11), leads to the following decomposition of the excess free energy

$$F^{\text{ex}} = F^{\text{ex,h}} + F_{\text{el}}^{\text{ex,c}} + F_{\text{corr}}^{\text{ex,c}} \quad (21)$$

with the electrostatic part

$$\begin{aligned} F_{\text{el}}^{\text{ex,c}}[\underline{\rho}] &:= \frac{1}{2} \sum_{ij} \int_V d^3r \int_V d^3r' \varrho_i(\mathbf{r}) \varrho_j(\mathbf{r}') U_{ij}^c(\mathbf{r}, \mathbf{r}') \\ &= \frac{1}{2} \int_V d^3r \int_V d^3r' \frac{\varrho^Q(\mathbf{r}) \varrho^Q(\mathbf{r}')}{\|\mathbf{r} - \mathbf{r}'\|_\infty} \\ &= \frac{1}{2} \int_V d^3r \varrho^Q(\mathbf{r}) \psi(\mathbf{r}) \end{aligned} \quad (22)$$

and the correlation part

$$F_{\text{corr}}^{\text{ex,c}}[\underline{\varrho}] := \frac{1}{2} \sum_{ij} \int_V d^3r \int_V d^3r' \varrho_i(\mathbf{r}) \varrho_j(\mathbf{r}') U_{ij}^c(\mathbf{r}, \mathbf{r}') [\exp(-U_{ij}^h(\mathbf{r}, \mathbf{r}')) - 1 + \exp(-U_{ij}^h(\mathbf{r}, \mathbf{r}')) G_{ij}(\kappa(\mathbf{r}, \mathbf{r}'; [\underline{\varrho}]), \|\mathbf{r} - \mathbf{r}'\|_\infty)]. \quad (23)$$

Here, the local charge density

$$\varrho^Q(\mathbf{r}) := \sum_i Q_i \varrho_i(\mathbf{r}) \quad (24)$$

and the electrostatic potential

$$\psi(\mathbf{r}) := \int_V d^3r' \frac{\varrho^Q(\mathbf{r}')}{\|\mathbf{r} - \mathbf{r}'\|_\infty} \quad (25)$$

have been introduced. Note that, although the integrands in Eqs. (22) and (23) are undefined for $\mathbf{r} = \mathbf{r}'$, the *three-dimensional* integrals exist due to the $\|\mathbf{r} - \mathbf{r}'\|_\infty^{-1}$ asymptotics for $\|\mathbf{r} - \mathbf{r}'\|_\infty \rightarrow 0$. Since the integrand in Eq. (23) decays as $\|\mathbf{r} - \mathbf{r}'\|_\infty^{-6}$ for $\|\mathbf{r} - \mathbf{r}'\|_\infty \rightarrow \infty$, $F_{\text{corr}}^{\text{ex,c}}$ is well-defined for all finite system volumes V and the thermodynamic limit of the ratio $\frac{1}{V} F_{\text{corr}}^{\text{ex,c}}$ exists. According to the last expression in Eq. (22), the same statements are true for the electrostatic contribution $F_{\text{el}}^{\text{ex,c}}$ provided the electrostatic potential ψ is well-defined. For locally charge neutral systems ($\varrho^Q = 0$), e.g., for bulk phases, the latter holds because of Eq. (25). In the next subsection it is shown that ψ can also be calculated in systems with only lateral translational symmetry.

D. Planar geometry

By imposing suitable boundary conditions, we consider only systems with translational symmetry in the lateral x and y directions. Hence, in the absence of spontaneous symmetry breaking, all densities ϱ_i depend at most on the z coordinate. Since the thermodynamic limit of globally charge neutral systems of Coulomb interacting hard particles exists [46], i.e., the bulk free energy density depends neither on the shape nor on the boundaries of the system volume V , the following system volumes of size $2L \times 2L \times L$ are considered in the limit $L \rightarrow \infty$:

$$V(L) := A(L) \times \left[-\frac{L}{2}, \frac{L}{2}\right], \quad (26)$$

where $A(L)$ is a square in the x - y plane of side length $2L$ with periodic boundary conditions.

The electrostatic potential in Eq. (25) can be expressed as

$$\psi(z) = \int_{-\frac{L}{2}}^{\frac{L}{2}} dz' \varrho^Q(z') \int_{A(L)} d^2a' \frac{1}{\|(\mathbf{a}', z - z')\|_\infty}, \quad (27)$$

where \mathbf{a}' denotes a two-dimensional vector in the x - y plane. The inner integral in Eq. (27) leads to

$$\begin{aligned} & \int_{A(L)} d^2a' \frac{1}{\|(\mathbf{a}', z - z')\|_\infty} \\ &= \int_0^{|x-x'|} da' 8a' \frac{1}{|x-x'|} + \int_{|x-x'|}^L da' 8a' \frac{1}{a'} \\ &= -4|x-x'| + 8L. \end{aligned} \quad (28)$$

In conjunction with the global charge neutrality constraint of Eq. (6), Eq. (27) reduces to

$$\psi(z) = -4 \int_{-\frac{L}{2}}^{\frac{L}{2}} dz' \varrho^Q(z') |z - z'|. \quad (29)$$

By differentiating twice, one finds that ψ fulfills the Poisson equation: $\psi'' = -8\varrho^Q$. Furthermore, by making use of global charge neutrality (Eq. (6)), one finds

$$\begin{aligned} \psi\left(-\frac{L}{2}\right) &= -4 \int_{-\frac{L}{2}}^{\frac{L}{2}} dz' \varrho^Q(z') \left(z' + \frac{L}{2}\right) \\ &= -4 \int_{-\frac{L}{2}}^{\frac{L}{2}} dz' \varrho^Q(z') z' \\ &= 4 \int_{-\frac{L}{2}}^{\frac{L}{2}} dz' \varrho^Q(z') \left(\frac{L}{2} - z'\right) \\ &= -\psi\left(\frac{L}{2}\right). \end{aligned} \quad (30)$$

Thus, the density functional in Eq. (3) takes the final form

$$\begin{aligned} \Omega[\underline{\varrho}] &= 4L^2 \sum_i \int_{-\frac{L}{2}}^{\frac{L}{2}} dz \varrho_i(z) \left(\ln(\varrho_i(z)) - 1 - \mu_i^*\right) \\ &\quad + \frac{1}{2} Q_i \psi(z) + F^{\text{ex,h}}[\underline{\varrho}] + F_{\text{corr}}^{\text{ex,c}}[\underline{\varrho}] \end{aligned} \quad (31)$$

which has to be minimized under the constraint of global charge neutrality (Eq. (6)). This is carried out by numerically solving the Euler-Lagrange equations (Eq. (7)) with a Picard-iteration scheme on a one-dimensional grid.

In the isotropic and nematic bulk fluid, the densities ϱ are spatially constant. In this case, the Euler-Lagrange equations Eq. (7) comprise five coupled equations:

$$\ln(\varrho_i^{(\text{bulk})}) - \mu_i^{*(\text{bulk})} - c_i^{\text{h},(\text{bulk})} - c_{\text{corr},i}^{\text{c},(\text{bulk})} = 0, \quad (32)$$

where the chemical potentials $\mu_i^{*(\text{bulk})}$ fulfill Eq. (5) and the local charge neutrality condition ($\sum_i Q_i \varrho_i^{(\text{bulk})} = 0$). The electrostatic contribution $-c_{\text{el},i}^{\text{c},(\text{bulk})} = Q_i \psi^{(\text{bulk})}$ is absent in Eq. (32) because the electrostatic potential ψ vanishes in locally charge neutral systems (see Eq. (25)).

For determining the number density profiles at free interfaces between coexisting bulk phases \mathcal{B}_1 and \mathcal{B}_2 , the Euler-Lagrange equations

$$\ln(\varrho_i(z)) - \mu_i^* + Q_i \psi(z) - c_i^{\text{h}}(z) - c_{\text{corr},i}^{\text{c}}(z) = 0 \quad (33)$$

are to be solved with the boundary conditions

$$\varrho_i \left(z = -\frac{L}{2} \right) = \varrho_i^{(\mathcal{B}_1)}, \quad \varrho_i \left(z = \frac{L}{2} \right) = \varrho_i^{(\mathcal{B}_2)}. \quad (34)$$

In order that for $z = -\frac{L}{2}$ and $z = \frac{L}{2}$ Eq. (33) reduces to Eq. (32) for \mathcal{B}_1 and \mathcal{B}_2 , respectively, one has the requirements

$$\begin{aligned} -\mu_i^* + Q_i \psi \left(-\frac{L}{2} \right) &= -\mu_i^{*(\mathcal{B}_1)}, \\ -\mu_i^* + Q_i \psi \left(\frac{L}{2} \right) &= -\mu_i^{*(\mathcal{B}_2)}. \end{aligned} \quad (35)$$

Using Eq. (30), one readily concludes

$$\mu_i^* = \frac{1}{2} \left(\mu_i^{*(\mathcal{B}_1)} + \mu_i^{*(\mathcal{B}_2)} \right) \quad (36)$$

and

$$\psi_D := \psi \left(\frac{L}{2} \right) - \psi \left(-\frac{L}{2} \right) = \frac{1}{Q_i} \left(\mu_i^{*(\mathcal{B}_1)} - \mu_i^{*(\mathcal{B}_2)} \right). \quad (37)$$

ψ_D is known as *Donnan potential* [47] between the two bulk phases \mathcal{B}_1 and \mathcal{B}_2 . It maintains a density gradient of the mobile particles at the interface between two coexisting bulk phases. Its definition given above is unique, i.e., the rightmost expression is in fact independent of i due to Eq. (5), e.g.,

$$\begin{aligned} \frac{\mu_A^{*(\mathcal{B}_1)} - \mu_A^{*(\mathcal{B}_2)}}{Q_A} &= \frac{\left(\mu_{\text{CA}}^* - \mu_{\text{C}}^{*(\mathcal{B}_1)} \right) - \left(\mu_{\text{CA}}^* - \mu_{\text{C}}^{*(\mathcal{B}_2)} \right)}{-Q_{\text{C}}} \\ &= \frac{\mu_{\text{C}}^{*(\mathcal{B}_1)} - \mu_{\text{C}}^{*(\mathcal{B}_2)}}{Q_{\text{C}}}. \end{aligned} \quad (38)$$

III. BULK FLUID

As a first step in the investigation of the density functional developed in the last section, bulk phase diagrams

are determined for various macroion charges Q_{M} by solving the bulk Euler-Lagrange equations (32).

The macroion and the salt number densities are given by $\varrho_{\text{M}} := \varrho_{\text{M}_x} + \varrho_{\text{M}_y} + \varrho_{\text{M}_z}$ and $\varrho_{\text{S}} := \varrho_{\text{A}}$, respectively. In order to detect the formation of liquid crystalline phases of the macroions, the equilibrium nematic order parameter for the director oriented relative to the z -direction,

$$s_{\text{M}} := \frac{3}{2} \frac{\varrho_{\text{M}_z}}{\varrho_{\text{M}}} - \frac{1}{2} \in \left[-\frac{1}{2}, 1 \right], \quad (39)$$

and the equilibrium biaxial order parameter,

$$q_{\text{M}} := \frac{\varrho_{\text{M}_x} - \varrho_{\text{M}_y}}{\varrho_{\text{M}}}, \quad (40)$$

have been determined. The definition of s_{M} agrees with the well-known scalar liquid-crystal order parameter $S = \langle P_2(\cos \vartheta) \rangle = \frac{3}{2} \langle (\cos \vartheta)^2 \rangle - \frac{1}{2}$ because within the Zwanzig model only macroion orientations M_z parallel ($\cos \vartheta = 1$) and $\text{M}_{x,y}$ perpendicular ($\cos \vartheta = 0$) to the z -axis are possible. s_{M} vanishes in an isotropic phase ($\varrho_{\text{M}_x} = \varrho_{\text{M}_y} = \varrho_{\text{M}_z}$), whereas it is positive in a nematic phase with director parallel to the z -axis ($\varrho_{\text{M}_z} > \varrho_{\text{M}_x}, \varrho_{\text{M}_y}$). A discrimination of the orientation M_z leads to negative values of s_{M} .

It turned out that the biaxial order parameter q_{M} vanishes throughout the whole inspected range of reduced chemical potentials $\mu_{\text{C}_k\text{M}}^*$ and μ_{CA}^* , whereas the nematic order parameter s_{M} indicates either an isotropic fluid ($s_{\text{M}} = 0$) or a nematic fluid ($s_{\text{M}} > 0$).

Figure 2 shows phase diagrams for the parameters [34] (compare Fig. 1) $D_{\text{M}} = 20 \ell_{\text{B}} \approx 14 \text{ nm}$, $L_{\text{M}} = \ell_{\text{B}} \approx 0.72 \text{ nm}$, $D_{\text{S}} = \ell_{\text{B}} \approx 0.72 \text{ nm}$, $Q_{\text{S}} = -e$ with $Q_{\text{M}} = 0$, $Q_{\text{M}} = 0.25 Q_{\text{S}}$, $Q_{\text{M}} = 0.5 Q_{\text{S}}$, $Q_{\text{M}} = 0.75 Q_{\text{S}}$, and $Q_{\text{M}} = Q_{\text{S}}$ in terms of the macroion packing fraction $\eta_{\text{M}} = \varrho_{\text{M}} D_{\text{M}}^2 L_{\text{M}}$ and the salt density ϱ_{S} .

One isotropic phase (I) and one nematic phase (N) are found separated by first-order phase transitions. Whereas for coexisting phases η_{M} is always smaller in the isotropic phase than in the nematic phase, ϱ_{S} of coexisting phases is higher in the isotropic and lower in the nematic phase. A similar displacement of salt from regions of large concentrations of charged macroions is known as Donnan effect [47]. Whereas the original Donnan effect has been discovered in systems subdivided by membranes which are impermeable for macroions, here the density difference of the macroions occurs due to two coexisting bulk phases. As for the case of membrane equilibrium, here a Donnan potential ψ_D (Eq. (37)) maintains the density gradients between the coexisting phases. Figure 3 shows its dependence on the macroion charge Q_{M} and the salt density ϱ_{S} . ψ_D decreases with increasing salt density ϱ_{S} . This tendency is intuitively expected as the Donnan effect becomes more pronounced with increasing macroion charge whereas increasing the salt density gives rise to a stronger screening of the macroion charge. For fixed salt density ϱ_{S} well below $\approx 0.1 \text{ mM}$, ψ_D decreases

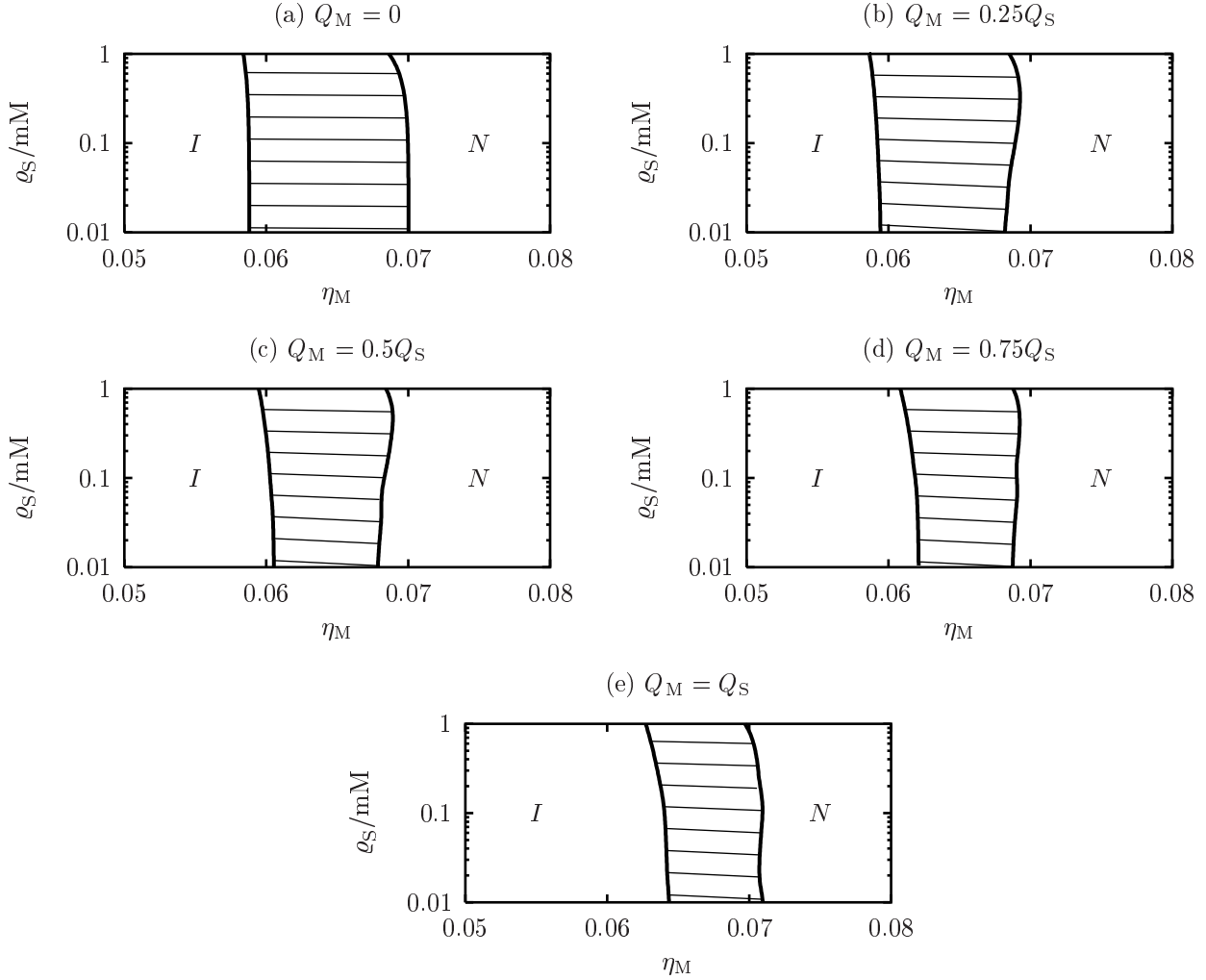


FIG. 2: Bulk phase diagrams of mixtures of plate-like macroions ($D_M = 20\ell_B$, $L_M = \ell_B$) and monovalent salt ($D_S = \ell_B$, $Q_S = -e$) for macroion charges $Q_M = 0$ (a), $Q_M = 0.25Q_S$ (b), $Q_M = 0.5Q_S$ (c), $Q_M = 0.75Q_S$ (d), and $Q_M = Q_S$ (e) in terms of the platelet packing fraction $\eta_M = \rho_M D_M^2 L_M$ and the salt density ρ_S [34]. Note that $\rho_S = 1$ mM for $D_S = 0.72$ nm corresponds to a salt packing fraction $\rho_S D_S^3 = 2.2 \cdot 10^{-4}$. Coexisting states are connected by (non-horizontal) tie lines. The model exhibits one isotropic (I) and one nematic (N) phase separated by first-order phase transitions. The salt density of coexisting phases is higher in the isotropic and lower in the nematic phase (Donnan effect) as can be inferred from the negative slope of the tie lines. For increasing macroion charge, the isotropic and the nematic binodals are shifted to larger macroion packing fractions η_M . With increasing salt density ρ_S , the isotropic-nematic binodals for systems of charged macroions bend towards lower values of the macroion packing fraction.

with increasing $|Q_M|$, whereas this behavior is reversed for fixed salt density ρ_S above ≈ 0.1 mM.

Upon an increase of the macroion charge $|Q_M|$, the isotropic and the nematic binodals are shifted to larger values of the macroion packing fraction η_M . This may be qualitatively understood by introducing the notion of an effective shape, which, in the present case, for macroions is given by a hard core surrounded by a soft $\|\cdot\|_\infty$ -sphere, i.e., a cube, with its linear extension proportional to Q_M^2 due to the pairwise Coulomb repulsion. For small macroion charges, the effective shape is still platelike whereas for highly charged colloids, the effec-

tive shape tends towards a cube leading to a shift of the two-phase region to larger macroion packing fractions.

For fixed macroion charge as well as particle shape and increasing salt density ρ_S , the isotropic-nematic binodals in Fig. 2 bend towards smaller macroion packing fractions. This behavior is expected intuitively, because high ionic strength causes strong screening which in turn leads to effectively quasi-hard platelets (see Fig. 2(a)).

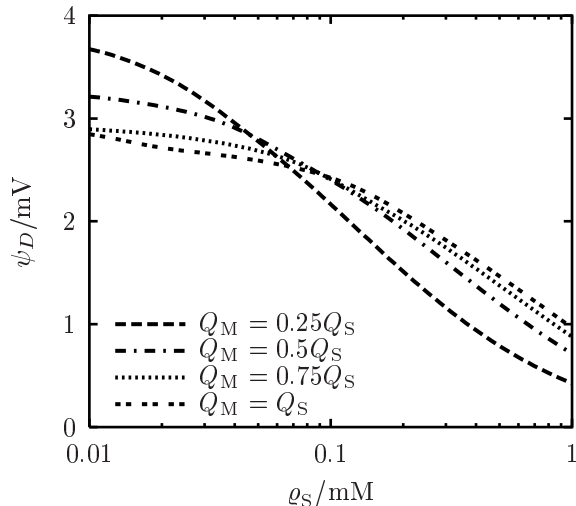


FIG. 3: Donnan potential ψ_D (see Eq. (37)) between the coexisting nematic (N) and isotropic (I) bulk phases in mixtures of platelike macroions and salt (see Fig. 2). For fixed macroion charge Q_M , the Donnan potential decreases with increasing salt density ρ_S . For salt densities $\rho_S \approx 0.01$ mM, ψ_D decreases with increasing $|Q_M|$, whereas for salt densities $\rho_S \approx 1$ mM, ψ_D increases with increasing $|Q_M|$.

IV. FREE INTERFACES

Based on the bulk properties provided in the previous section, we are now able to calculate the density profiles at the free interfaces between the coexisting isotropic and nematic phases by solving the spatially varying Euler-Lagrange equations (Eq. (33)). The density and order parameter profiles corresponding to the parameters used in the previous section (see also Figs. 2 and 3) and to nematic bulk salt density $\rho_S^{(N)} = 2.2 \cdot 10^{-5} \hat{=} 0.1$ mM [34] are depicted in Figs. 4 and 5, respectively. The interface position $z = 0$ is chosen such that $\varrho_M(0) = \frac{1}{2} (\varrho_M^{(I)} + \varrho_M^{(N)})$.

First, and most important, the formalism described in Sec. II renders stable free interfaces between coexisting bulk phases. This should be regarded as an accomplishment which can be traced back to using the spatially varying screening factor κ introduced in Eq. (16); trials with spatially constant κ were not successful.

For a given density profile $\varrho_M(z)$ (Fig. 4), the corresponding interface width ζ is defined as the spatial distance between the loci, where the tangent at the density profile at position $z = 0$ reaches the values of the nematic bulk density $\varrho_M^{(N)}$ and the isotropic bulk density $\varrho_M^{(I)}$, respectively. This interface width ζ decreases monotonically with increasing macroion charge from $\zeta = 1.8D_M$ for $Q_M = 0.25Q_S$ to $\zeta = 1.3D_M$ for $Q_M = Q_S$ (see Fig. 4). The Debye length κ^{-1} decreases monotonically from $\kappa^{-1} = 1.5D_M$ for $Q_M = 0.25Q_S$ to $\kappa^{-1} = D_M$ for $Q_M = Q_S$. Finally, the bulk correlation lengths ξ of

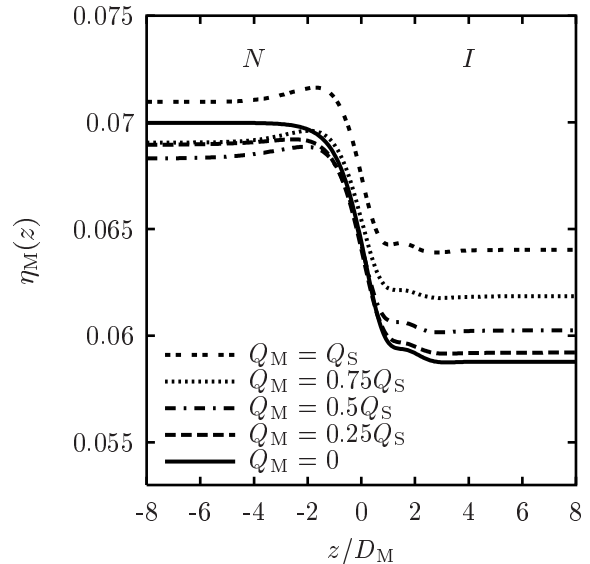


FIG. 4: Macroion density profiles at the free interface between coexisting isotropic (I) and nematic (N) phases for the mixtures of platelike macroions and salt as studied in Fig. 2 at nematic bulk salt density $\rho_S^{(N)} = 2.2 \cdot 10^{-5} \hat{=} 0.1$ mM [34]. The interface position $z = 0$ is chosen such that $\varrho_M(0) = \frac{1}{2} (\varrho_M^{(I)} + \varrho_M^{(N)})$. The interface width ζ , inferred from the slope of the density profiles at the interface position $z = 0$ (see main text), the Debye length κ^{-1} , and the bulk correlation lengths ξ , inferred from the exponential decay of the density profiles, decrease monotonically with increasing macroion charge $|Q_M|$. The same behavior is found for the interfacial tension γ . See also Fig. 5.

the coexisting isotropic and nematic bulk phases, inferred from the exponential decay lengths of $\varrho_M(z) - \varrho_M^{(I,N)}$, also decrease monotonically upon increasing $|Q_M|$ and the values are by and large equal to those of κ^{-1} .

The nematic order parameter profiles $s_M(z)$ (Fig. 5) interpolate almost monotonically between $s_M(\infty) > 0$ in the nematic bulk phase (N) and $s_M(\infty) = 0$ in the isotropic bulk phase (I). Note that s_M has been defined for a director in z -direction, i.e., platelets on the nematic side ($z < 0$) are preferably oriented parallel to the free interface. At a fixed position on the nematic side ($z < 0$), $s_M(z)$ decreases with increasing macroion charge $|Q_M|$. This behavior is consistent with the picture of an increasingly isotropic effective shape, introduced in the previous section.

The charge density profiles $\varrho^Q(z)$ (Eq. (24)) displayed in Fig. 6 show deviations from local charge neutrality within the interfacial region $-4D_M \lesssim z \lesssim 4D_M$. A negative charge density occurs on the nematic side (N) and a positive charge density on the isotropic side (I). Such a local charging is necessary for the appearance of the non-vanishing Donnan potentials ψ_D shown in Fig. 3. The full electrostatic potential profiles $\psi(z)$ are depicted in Fig. 7. They increase monotonically from

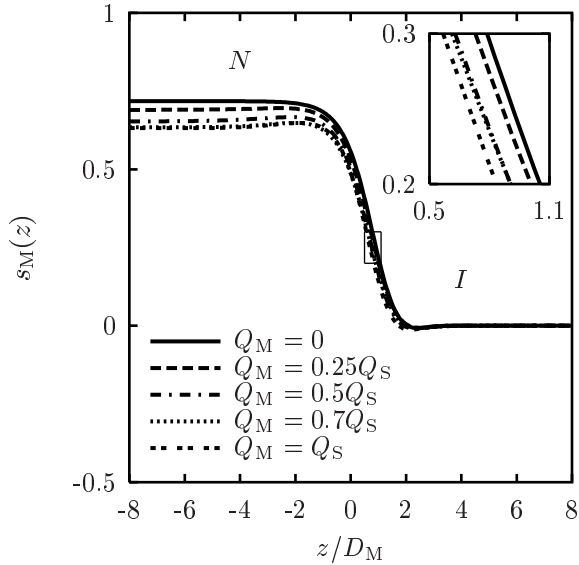


FIG. 5: Macroion nematic order parameter profiles s_M (Eq. (39)) at the free interface between coexisting isotropic (I) and nematic (N) phases for mixtures of platelike macroions and salt as shown in Fig. 2 at nematic bulk salt density $\varrho_S^{(N)} = 2.2 \cdot 10^{-5} \hat{=} 0.1 \text{ mM}$ [34]. The position $z = 0$ is fixed by the choice $\varrho_M(0) = \frac{1}{2} (\varrho_M^{(I)} + \varrho_M^{(N)})$ (see Fig. 4). On the nematic side of the free interface, most of the macroions lie parallel to the interface. For $z < 0$, $s_M(z)$ decreases with increasing macroion charge $|Q_M|$. The inset shows a detailed view of the steepest portions of the nematic order parameter profiles in the range $s_M(z) \in [0.2, 0.3]$ indicated by the frame.

the macroion-rich nematic phase N to the macroion-poor isotropic phase I , maintaining the density gradients occurring in the interface region. The potential difference $\psi(\infty) - \psi(-\infty)$ equals the Donnan potential ψ_D (see Eq. (37) and Fig. 3).

The interfacial tensions γ of the interfaces shown in Fig. 4 decrease monotonically from $\gamma = 1.33 \cdot 10^{-5} \hat{=} 108 \text{ nN} \cdot \text{m}^{-1}$ for $Q_M = 0.25Q_S$ to $\gamma = 6 \cdot 10^{-7} \hat{=} 5 \text{ nN} \cdot \text{m}^{-1}$ for $Q_M = Q_S$ [34], which are comparable to experimental findings for laponite suspensions [16]. The corresponding wetting parameters $\omega = (4\pi\gamma\xi^2)^{-1}$ [48] are in the range $6 \dots 340$. If these values for γ are indeed so small, the free isotropic-nematic interfaces are expected to be strongly affected by capillary wavelike fluctuations which are not captured by the present theory.

Calculating bulk phase diagrams and density profiles for macroion charges $Q_M \geq 1.25Q_S$ along the lines described above lead to unphysical results like, e.g., negative interfacial tensions. The reason for this phenomenon is that the bulk phases determined in Sec. III are assumed to be spatially homogeneous, whereas it can be shown that the equilibrium bulk states are spatially inhomogeneous for sufficiently large macroion charges (see Subsec. II C).

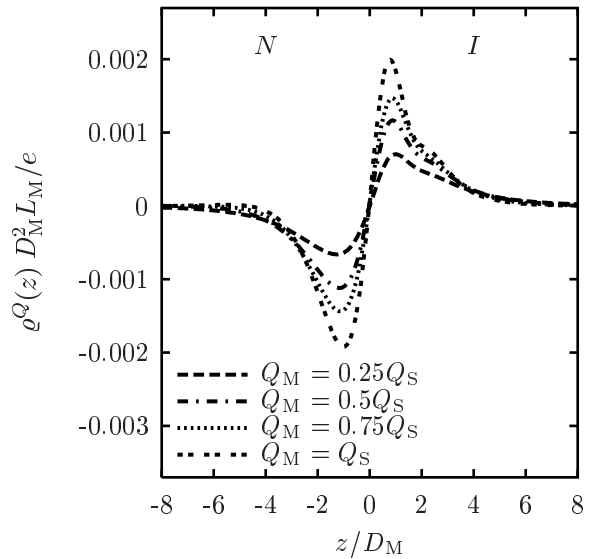


FIG. 6: Local charge density profiles (Eq. (24)) at the free isotropic-nematic interfaces shown in Figs. 4 and 5 using the same parameters and line code. Whereas *global* charge neutrality holds, deviations from *local* charge neutrality occur near the interface with a negative charge density on the nematic side (N) and a positive charge density on the isotropic side (I). The corresponding electrostatic potential profile is shown in Fig. 7.

V. DISCUSSION AND SUMMARY

The numerical results for the bulk systems and the free interfaces presented in Secs. III and IV, respectively, are in good qualitative agreement with intuitive expectations. Within the density functional theory described in Sec. II one gains access not only to interfacial density profiles at free interfaces between coexisting bulk phases but also to local charge densities and electrostatic potential profiles.

Since here we have been interested in spatially homogeneous (isotropic or nematic) bulk phases, only very small macroion charges ($|Q_M| \leq e$) have been considered. Determining phase coexistence for larger platelet charges is computationally more demanding because spatially inhomogeneous bulk phases are involved. Note that, according to Subsec. II C, charges have to be interpreted as effective charges.

A further difficulty related to the choice of the pair distribution functions $g_{ij}^{(\eta)}$ used in Eq. (11) may appear if, as for Eq. (15), the effective shape of the macroions becomes more and more isotropic upon increasing the macroion charge: In this case, the two-phase region between isotropic and anisotropic phase is shifted to unrealistically large packing fractions. Therefore, the pair distribution functions must be chosen properly in order to yield *anisotropic* effective macroion shapes up to large macroion charges. Unfortunately, deriving *analytical* expressions for pair distribution functions of platelike par-

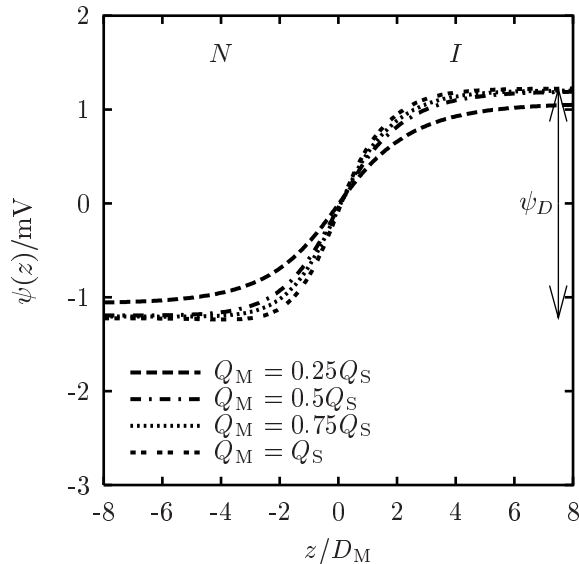


FIG. 7: Electrostatic potential profiles at the free isotropic-nematic interfaces shown in Figs. 4-6. The potential difference between the nematic and the isotropic bulk is given by the Donnan potential ψ_D displayed in Fig. 3; it is indicated for $Q_M = Q_S$.

ticles with inhomogeneous charge distributions is still a big challenge.

In conclusion, the density-functional theory of charged platelike particles developed here can be regarded as a first step to understand qualitatively free interfaces be-

tween isotropic and nematic bulk phases of suspensions of charged platelets and salt. Here, we have constructed a density functional for charged platelike particles and applied it to a ternary mixture of platelike macroions and salt ions (Fig. 1) in the bulk and at free interfaces between coexisting isotropic and nematic phases. For sufficiently small macroion charges, the bulk phase diagrams in terms of densities (Fig. 2) exhibit one isotropic phase and one nematic phase. For increasing macroion charge and fixed salt densities, the two-phase coexistence region is shifted to larger macroion packing fractions. For fixed macroion charge and increasing salt density, the limit of quasi-hard platelets is approached. The Donnan potential between coexisting phases (Fig. 3) can be expressed in terms of the particle chemical potentials gained from bulk structure calculations. Density and nematic order parameter profiles at free interfaces between isotropic and nematic phases at coexistence (Figs. 4 and 5) show non-monotonic behavior. The value of the nematic order parameter in the nematic bulk phase decreases upon increasing the macroion charge. The width of the interface and the bulk correlation lengths are approximately given by the Debye length. The interfacial tension decreases upon increasing the macroion charges. Electrically charged layers form at the free interface (Fig. 6). The corresponding electrostatic potential profiles (Fig. 7) exhibit monotonic behavior. Investigations of spatially inhomogeneous bulk phases are necessary in order to apply the theory to larger macroion charges. Improvements of the present theory call for more accurate analytical expressions for the pair distribution function between charged platelike particles.

-
- [1] P. Davidson and J.-Ch.P. Gabriel, *Curr. Opin. Colloid Interface Sci.* **9**, 377 (2005).
 - [2] I. Langmuir, *J. Chem. Phys.* **6**, 873 (1938).
 - [3] British Ceramic Society, *Clay and other colloidal systems* (Proc. Brit. Ceramic Soc. **13**) (British Ceramic Society, Stoke-on-Trent, 1969).
 - [4] A. Mourchid, A. Delville, J. Lumbard, E. Lécolier, and P. Levitz, *Langmuir* **11**, 1942 (1995).
 - [5] J.-Ch.P. Gabriel, C. Sanchez, and P. Davidson, *J. Phys. Chem.* **100**, 11139 (1996).
 - [6] F. Pignon, A. Magnin, J.-M. Piau, B. Cabane, P. Lindner, and O. Diat, *Phys. Rev. E* **56**, 3281 (1997).
 - [7] M. Kroon, W.L. Vos, and G.H. Wegdam, *Phys. Rev. E* **57**, 1962 (1998).
 - [8] A. Mourchid, E. Lécolier, H. van Damme, and P. Levitz, *Langmuir* **14**, 4718 (1998).
 - [9] J.M. Saunders, J.W. Goodwin, R.M. Richardson, and B. Vincent, *J. Phys. Chem. B* **103**, 9211 (1999).
 - [10] P. Levitz, E. Lécolier, A. Mourchid, A. Delville, and S. Lyonnard, *Europhys. Lett.* **49**, 672 (2000).
 - [11] T. Nicolai and S. Cocard, *Langmuir* **16**, 8189 (2000).
 - [12] T. Nicolai and S. Cocard, *Eur. Phys. J. E* **5**, 221 (2001).
 - [13] P. Porion, M. Al Mukhtar, S. Meyer, A.M. Faugère, J.R.C. van der Maarel, and A. Delville, *J. Phys. Chem. B* **105**, 10505 (2001).
 - [14] P. Porion, M. Al-Mukhtar, A.-M. Faugère, S. Meyer, and A. Delville, *Eur. Phys. J. E* **12**, S17 (2003).
 - [15] F.M. van der Kooij and H.N.W. Lekkerkerker, *J. Phys. Chem. B* **102**, 7829 (1998).
 - [16] F.M. van der Kooij, D. van der Beek, and H.N.W. Lekkerkerker, *J. Phys. Chem. B* **105**, 1696 (2001).
 - [17] D. van der Beek and H.N.W. Lekkerkerker, *Europhys. Lett.* **61**, 702 (2003).
 - [18] D. van der Beek and H.N.W. Lekkerkerker, *Langmuir* **20**, 8582 (2004).
 - [19] A.B.D. Brown, S.M. Clarke, and A.R. Rennie, *Langmuir* **14**, 3129 (1998).
 - [20] A.B.D. Brown, C. Ferrero, T. Narayanan, and A.R. Rennie, *Eur. Phys. J. B* **11**, 481 (1999).
 - [21] S. Dietrich and A. Haase, *Phys. Rep.* **260**, 1 (1995).
 - [22] C.D. Bain, *Curr. Opin. Colloid Interface Sci.* **3**, 287 (1998).
 - [23] R. Zwanzig, *J. Chem. Phys.* **39**, 1714 (1963).
 - [24] R. Evans, *Adv. Phys.* **28**, 143 (1979).
 - [25] L. Harnau and S. Dietrich, *Phys. Rev. E* **65**, 021505 (2002).
 - [26] L. Harnau and S. Dietrich, *Phys. Rev. E* **66**, 051702 (2002).

- [27] M. Bier, L. Harnau, and S. Dietrich, Phys. Rev. E **69**, 021506 (2004).
- [28] P. Debye and E. Hückel, Phys. Z. **24**, 185 (1923).
- [29] L. Harnau, D. Costa, and J.-P. Hansen, Europhys. Lett. **53**, 729 (2001).
- [30] L. Harnau and J.-P. Hansen, J. Chem. Phys. **116**, 9051 (2002).
- [31] I.S. Sogami, T. Shinohara, and M.V. Smalley, Mol. Phys. **74**, 599 (1991).
- [32] D.G. Rowan, J.-P. Hansen, and E. Trizac, Mol. Phys. **98**, 1369 (2000).
- [33] E. Trizac, L. Bocquet, A. Agra, J.-J. Weis, and M. Aubouy, J. Phys.: Condens. Matter **14**, 9339 (2002).
- [34] Dimensionless quantities are used in units of $\beta^{-1} = k_B T$ (thermal energy), e (proton charge), and $\ell_B = \frac{\beta e^2}{4\pi\epsilon_0\epsilon}$ (Bjerrum length) with the solvent dielectric constant ϵ . For $T = 300$ K and $\epsilon = 78$ (water) the latter is $\ell_B \approx 0.72$ nm. In order to avoid a clumsy notation, the corresponding dimensional quantities are denoted by the same symbol and can be recognized by the presence of units. Dimensional number densities are sometimes given in units of $1 \text{ mM} = 1 \text{ mol} \cdot \text{m}^{-3} \approx 6 \cdot 10^{23} \text{ m}^{-3}$.
- [35] J.A. Cuesta and Y. Martínez-Ratón, Phys. Rev. Lett. **78**, 3681 (1997).
- [36] J.A. Cuesta and Y. Martínez-Ratón, J. Chem. Phys. **107**, 6379 (1997).
- [37] D.A. McQuarrie, *Statistical Mechanics* (University Science Books, Sausalito, 2000).
- [38] J.P. Hansen and I.R. McDonald, *Theory of simple liquids* (Academic, Amsterdam, 1986).
- [39] B.P. Lee and M.E. Fisher, Europhys. Lett. **39**, 611 (1997).
- [40] M. Aubouy, E. Trizac, and L. Bocquet, J. Phys. A **36**, 5835 (2003).
- [41] P.B. Warren, J. Chem. Phys. **112**, 4683 (2000).
- [42] L. Onsager and N.N.T. Samaras, J. Chem. Phys. **2**, 528 (1934).
- [43] B. Groh, R. Evans, and S. Dietrich, Phys. Rev. E **57**, 6944 (1998).
- [44] I.S. Gradshteyn and I.M. Ryzhik, *Table of integrals, series, and products* (Academic, New York, 1980).
- [45] M. Abramowitz and I.S. Stegun, *Handbook of mathematical functions* (Dover, New York, 1972).
- [46] E.H. Lieb and J.L. Lebowitz, Adv. Math. **9**, 316 (1972).
- [47] A.W. Adamson, *A textbook of physical chemistry* (Academic, New York, 1973).
- [48] M. Schick, in *Les Houches, Session XLVIII, 1988 — Liquides aux interfaces / Liquids at interfaces*, edited by J. Charvolin, J.F. Joanny, and J. Zinn-Justin (North-Holland, Amsterdam, 1990), p. 415.